Optical Materials: X 25 (2025) 100394

Contents lists available at ScienceDirect

Optical Materials: X

journal homepage: www.journals.elsevier.com/optical-materials-x

# Influence of short-pulsed Ion irradiation on optical and photoelectrical properties of thin gallium oxide films

Zhanymgul Koishybayeva [a,*], Fedor Konusov [b], Sergey Pavlov [b], Dmitrii Sidelev [b], Artur Nassyrbayev [b], Dmitry Cheshev [b], Ruslan Gadyrov [c], Vladislav Tarbokov [b], Abdirash Akilbekov [a]

[a] L.N. Gumilyov Eurasian National University, 2 Satpayev Str., 010008, Astana, Kazakhstan
[b] National Research Tomsk Polytechnic University, 30 Lenina Ave., 634050, Tomsk, Russia
[c] National Research Tomsk State University, 36 Lenina Ave., 634050, Tomsk, Russia

ARTICLE INFO

*Keywords:*
Gallium oxide
Thin films
Radiation resistance
Magnetron sputtering
Short-pulsed ion irradiation
Radiation defects
Optical properties

ABSTRACT

In this work the influence of a short-pulsed ion irradiation with a high flux (~5.5•$10^{19}$ $cm^{-2}s^{-1}$) on structure, optical and photo-electrical properties of gallium oxide thin films have been investigated. The films were produced by the radio-frequency magnetron sputtering method. A part of deposited films was annealed in the air environment (900 °C, 2 h) for synthesis of β-$Ga_2O_3$ phase. Obtained films were subjected to the short-pulsed ion irradiation (ion energy - up to 200 keV, pulse duration - 90 ns, current density on the target - up to 15 A/$cm^2$). The influence of the annealing and the irradiation on spectral dependences of absorption, the bandgap width and the Urbach energy have been determined. It was found that irradiation leads to amorphization of crystalline β-$Ga_2O_3$ films and a significant change in optical characteristics. In addition, we measured the magnitude of surface dark and photoconductivity of the films. Also, the field and spectral dependences of the photosensitivity of the films were researched. As a result, it was established that short-pulsed irradiation improves the photoelectric properties of amorphous gallium oxide films. The reasons of it are discussed.

## 1. Introduction

Gallium oxide of monoclinic modification β-$Ga_2O_3$ has a bandgap width of 4.9 eV and is a promising material for various electronic and optoelectronic devices, including field-effect transistors, solar cell elements, solar blind UV photodetectors, scintillators, and dosimetry materials [1–11]. Thin films of β-$Ga_2O_3$ could be produced by various methods such including sol-gel, chemical vapor deposition, molecular beam epitaxy, pulsed laser deposition and magnetron sputtering methods. Considering the potential applications of such structures, radiation resistance and stability of optical and photoelectrical properties when exposed to ionizing radiation fluxes are of significant importance. Extensive previous studies of the effects of radiation exposure of β-$Ga_2O_3$-based devices by electrons, protons, and neutrons, and found that β-$Ga_2O_3$ has comparable radiation resistance to conventional wide-gap semiconductors [1,12]. Moreover, ion irradiation can be used to modify the photoelectrical properties of thin films. Thus, in work [13] it is shown that irradiation with 5 MeV protons of MOCVD grown β-$Ga_2O_3$ thin films increases the photocurrent, but decreases the photo-to-dark current ratio. At the same time, the dose rate and irradiation temperature can have an important effect on the accumulation of radiation induced disorder as was shown in Ref. [14] for the irradiation of β-$Ga_2O_3$ single crystals by $Ni^+$ ions in a wide range of ion fluxes (8 × $10^{10}$–5 × $10^{12}$ $cm^{-2}s^{-1}$) and irradiation temperatures (25–300 °C).

In this paper, we investigated the effect of short-pulsed ion irradiation by $C^+/H^+$ ion beam with a high flux (~5.5•$10^{19}$ $cm^{-2}s^{-1}$) on the structure, optical characteristics and photoconductivity of amorphous and polycrystalline gallium oxide films deposited on sapphire substrates

This paper was presented at the 12th International Conference on Luminescent Detectors and Transformers of Ionizing Radiation (LUMDETR), June 16-21, 2024, Riga, Latvia.

* Corresponding author.
*E-mail addresses:* zhanymgul.k@gmail.com (Z. Koishybayeva), konusov@tpu.ru (F. Konusov), lab.sergey@gmail.com (S. Pavlov), sidelevdv@tpu.ru (D. Sidelev), arn1@tpu.ru (A. Nassyrbayev), dimascabal@gmail.com (D. Cheshev), grm882@ngs.ru (R. Gadyrov), tarbokovv@tpu.ru (V. Tarbokov), akilbekov_at@enu.kz (A. Akilbekov).

https://doi.org/10.1016/j.omx.2024.100394
Received 29 October 2024; Received in revised form 8 December 2024; Accepted 15 December 2024
Available online 19 December 2024

by magnetron sputtering.

## 2. Materials and methods

The deposition of gallium oxide thin films was performed by radio-frequency (RF) magnetron sputtering. Polished α-$Al_2O_3$ sapphire plates with (0001) orientation were used as substrates. The substrates have been subjected to ultrasound cleaning in alcohol, then dried in a compressed air, then mounted on a planetary substrate holder. The residual pressure in the chamber was $2 \times 10^{-3}$ Pa. Before the deposition, the substrates have etched with an argon ion beam using an ion source (accelerating voltage - 3 kV, ion current - 45 mA, argon pressure - 0.12 Pa) for 15 min. Further, the film deposition was performed by sputtering a polycrystalline $Ga_2O_3$ target (diameter - 90 mm, purity - 99.9 %) at RF power of 300 W in a mixture of argon and oxygen (the flow ratios were 20/18 sccm). The deposition time was 90 min. The thickness of the deposited films was 400 nm according to cross-section electron microscopy measurements.

A part of samples were annealed in a muffle furnace in air at 900 °C for 2 h after the deposition. The temperature in the chamber was controlled by a platinum-rhodium thermocouple.

The films were irradiated by ion beam using a TEMP-4M accelerator in the mode of the short-pulsed ion irradiation [15]. The parameters of the ion beam were the following: beam composition – carbon ions (80–85 %) and protons (15–20 %), the accelerating voltage is 200 kV, the ion current density on the target $j = 8$–$15$ A/cm$^2$, the pulse duration is 90 ns and the flux of ions Φ is about $5 \times 10^{12}$ cm$^{-2}$ per pulse. Number of pulses was 3, 30 and 150.

The phase composition of the materials was studied by X-ray diffractometry (XRD) and Raman spectroscopy methods. XRD was performed using a Shimadzu XRD-7000 X-ray diffractometer with CuKα$_1$ radiation ($\lambda_1 = 1.5406$ Å) with step scanning in the range of $2\theta = 10°$–$90°$ in the Bragg-Brentano geometry, as well as in the grazing geometry (GXRD) to suppress substrate reflections at an incidence angle of the beam of $\theta = 3°$. Identification of diffraction peaks was carried out using the Crystallographica Search-Match program and the PDF4+ structural database. X-ray structural analysis was carried out using the PowderCell 2.4 program using the PDF4+ structural database. Raman spectra were recorded using NTEGRA NT-MDT AFM-Raman system with 532 nm laser and 100× objective.

Optical density spectra were measured by Avantes Avaspec 2048 spectrometer. The spectral dependences of the absorption coefficient α(h$\nu$) of the films were calculated from the spectral dependences of the optical density using the formula $\alpha(h\nu) = D(h\nu)/d$, where $d$ is the thickness of the films, $D(h\nu)$ is the difference between the optical density of the film on the substrate and the optical density of the substrate. The spectra $\alpha(h\nu)$ were approximated by the Urbach rule [16] in the energy intervals $\Delta(h\nu)$, in which ln α ∝ $h\nu$:

$$\alpha(h\nu) \propto \exp(h\nu / E_U), \quad (1)$$

where $E_U$ is the Urbach energy. The bandgap width $E_g$' was determined using approximation of the absorption spectra by the power law:

$$(\alpha \times h\nu) \propto (h\nu - E_g')^{0.5}. \quad (2)$$

Induced absorption was calculated using the difference $\Delta\alpha(h\nu) = \alpha_i(h\nu) - \alpha_0(h\nu)$ where $\alpha_0$ is absorption coefficient before and $\alpha_i$ is that after irradiation. The defects concentration before $N_0$ and after irradiation $N_i$ was calculated from the spectra according to the Smakula equation [17]:

$$N_{0(i)} = 0.87 \times 10^{17} \times \frac{n}{(n+2)^2} \times \frac{\gamma}{f} \times \alpha'_0, \quad (3)$$

where $n$ is the refractive index, $f$ is the strength of the transition oscillator (in this work, we take $f = 1$ to estimate the lower limit of the defect concentration), and $\alpha'_0$ is the absorption coefficient at the maximum of local band centered at $h\nu_0$ and half width γ. At that we used the dependency $n(h\nu)$ calculated from the interference pattern of spectra. The rate of radiation defects (RDs) generation was found by the formula:

$$\Delta N_i / \Delta\Phi = (N_{i2} - N_{i1}) / (\Phi_2 - \Phi_1), \quad (4)$$

where $N_{i1,2}$ are the RDs concentrations at ion fluences $\Phi_{1,2}$.

The photoluminescence spectra $I_{PL}(h\nu)$ were measured using Solar CM 2203 spectrofluorometer in the range of $h\nu = 1.5$–$3.5$ eV at an energy of the excitation radiation of 4.96 eV.

The measurement of surface dark $\sigma_d$ and photoconductivity $\sigma_{ph}$ was carried out in air in a two-electrode scheme with pair of copper overlay electrodes with a length of 0.5 cm at spacing of 0.2–0.3 cm. Radiation from a mercury lamp with lines at photon energies of 4.89, 3.96, 3.4, 3.06, 2.85, 2.27 eV, and 2.17 eV was used to excite photoconductivity, using broadband interference filters to highlight regions of selective photosensitivity of the film material.

## 3. Results and discussions

### 3.1. Influence of ion irradiation on material's structure

Phase composition of the films was investigated by Raman spectroscopy and XRD. After deposition, the coatings possess an amorphous structure (Figs. 1 and 2). Due to annealing a β-$Ga_2O_3$ phase in the coating was formed which is evidenced by active $A_g^{(3)}$ (201 cm$^{-1}$) and $A_g^{(5)}$ (348 cm$^{-1}$) phonon modes [18] (Fig. 1) and corresponding reflexes on X-ray diffraction pattern (Fig. 2). Lattice parameters are determined as $a = 12.2343$, $b = 3.0317$ and $c = 5.8003$. The crystallite size estimate is about 20 nm. According to the results no other gallium oxide phases in the coatings were formed after annealing.

Irradiation in the short-pulse implantation mode resulted in amorphization of the films (Figs. 1 and 2). Considering the not significant ion fluxes during experiments (up to $7.5 \times 10^{14}$ cm$^{-2}$), we suggest that the film amorphization take place due to conjoint action of pulsed heating and intense radiation damage [15,19].

### 3.2. Optical absorption

#### 3.2.1. Optical characteristics before irradiation

The spectra $\alpha(h\nu)$ of the deposited films are characterized by fundamental absorption edge at $h\nu > 4.5$ eV (Fig. 3) The bandgap (BG) of direct allowed transitions in the deposited films is $E_g$' = 4.97–5.05 eV,

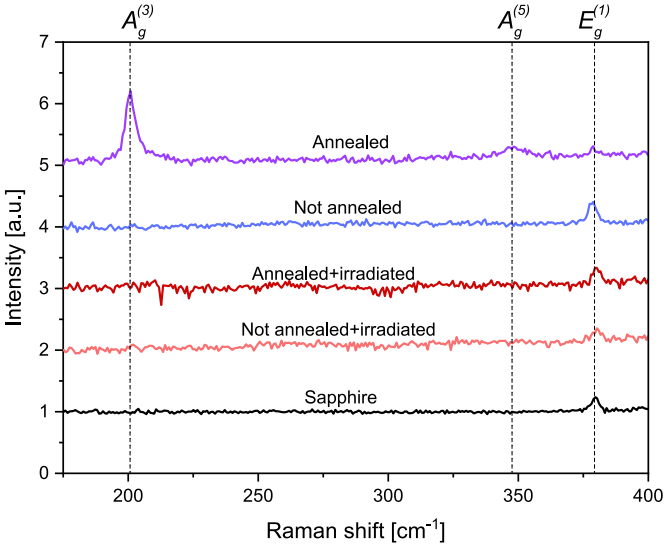


**Fig. 1.** Raman spectra from sapphire substrate and samples with coatings before and after annealing and irradiation. Spectra have offset.

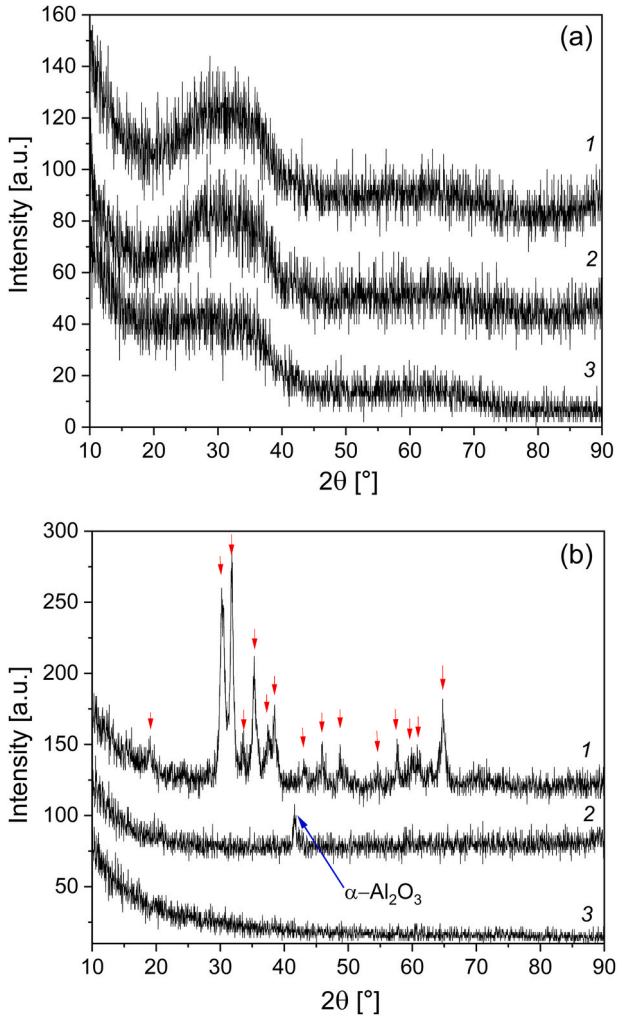


**Fig. 2.** X-ray diffraction patterns of samples before (a) and after (b) annealing, before (1) and after irradiation (2,3). Curves (3) were taken in GXRD mode. The red arrows mark the positions of the reflexes corresponding to the β-$Ga_2O_3$ phase according to JCPDS card No. 41–1103.

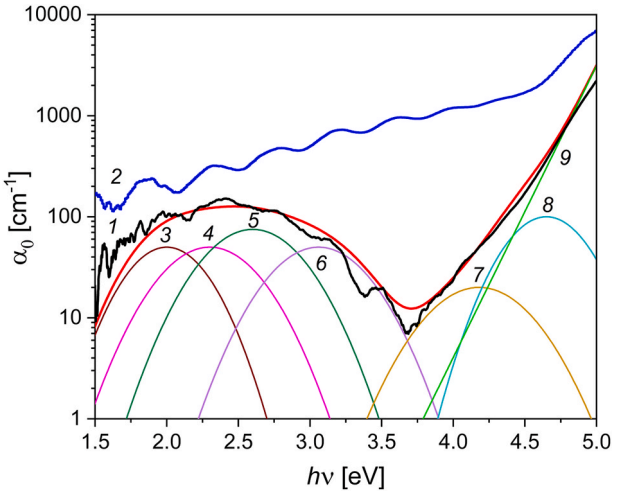


**Fig. 3.** Spectral dependences of the absorption coefficient α(*hν*) of gallium oxide films before (*1*) and after (*2*) annealing and decomposition of curve (*1*) by Gaussians (*3–8*) with centers at $h\nu_0$ and half-width of γ: $h\nu_0$ = 2.0 eV and γ = 0.25 eV (*3*), 2.3 eV and 0.3 eV (*4*), 2.6 eV and 0.3 eV (*5*), 3.06 eV and 0.3 eV (*6*), 4.2 eV and 0.32 eV (*7*) and 4.65 and 0.25 eV (*8*) eV. Curve (*9*) shows the fitting of absorption edge using Urbach rule with parameters $\alpha_{00} = 1 \times 10^{-11}$ $cm^{-1}$ and $E_U$ = 0.15 eV.

which is close to values of crystalline β-$Ga_2O_3$ (Table 1) [20–26]. However, after annealing at 900 °C in air, the bandgap width narrows to $E_g$' = 4.77–4.79 eV. The Urbach energy for the states of growth defects (GDs) localized in the bandgap in the range of 4.0–5.0 eV after annealing, therefore, increases from $E_U$ = 0.2–0.25 eV to 0.3–0.35 eV due to the enhancing of interaction between defects at the overlap of their levels. Such change in absorption edge characteristics can be determined by the oxygen content of the films and is due to the cooperation of $V_O$ vacancy levels into the subzone, as demonstrated before [26,27]. Moreover, the values $E_U$ = 0.5 eV and $E_g$' = 4.0–4.5 eV are characteristic of amorphous a-$GaO_x$ films [26], that indicates a higher defect concentration in a film structure. α(*hν*) spectra of the deposited films has a wide absorption band in the range of 1.6–3.4 eV due to transitions involving local levels of intrinsic GDs (Fig. 3). The annealing process stimulates the transformation of local bands into a continuous distribution of energy levels of exponential form in the range of 1.4–4.6 eV with an Urbach energy of $E_U$ = 1.2–1.5 eV (Fig. 3). Such transformation of the absorption spectrum is due to the formation of complexes from intrinsic vacancy defects with the participation of oxygen atoms (or molecules) under the influence of annealing. Decomposition of the spectra of amorphous films into elementary Gaussians revealed local bands with centers at $h\nu_0$ = 2.0 eV, 2.3 eV, 2.6 eV, 3.06 eV, 4.2 eV and 4.65 eV and calculated concentration of GDs $N = 6.6 \times 10^{16}$ $cm^{-3}$, $7.9 \times 10^{16}$ $cm^{-3}$, $1.2 \times 10^{17}$ $cm^{-3}$, $7.9 \times 10^{16}$ $cm^{-3}$, $3.4 \times 10^{16}$ $cm^{-3}$ and $1.3 \times 10^{17}$ $cm^{-3}$ respectively (Fig. 3). The absorption edge was calculated using Urbach rule at $E_U$ = 0.15 eV (Fig. 3). The absorption bands in β-$Ga_2O_3$ are usually associated with electronic transitions between the local levels of anionic $V_O$ and cationic $V_{Ga}$ vacancies and the bottom of the conduction band (CB) $\varepsilon_c$ or the top of the valence band (VB) $\varepsilon_v$ [20–25]. The band at 2.0 eV can be attributed to transitions from the donor level $\varepsilon_c$–2.0 eV of the $V_O$ + vacancy in the CB [20,21]. The 2.3 eV band can be formed due to transitions from VB to the acceptor level $\varepsilon_v$+2.3 eV of $V_{Ga}$ [20–23]. The contribution to the band at 2.6 eV may be made by transitions from the VB to the level $\varepsilon_v$+2.6 eV of the $V_{Ga}$ + [20–23]. The band at 3.06 eV is most probably formed by transitions from the VB to level $\varepsilon_v$+3.06 eV of the $V_{Ga}$ [20,22]. The short-wavelength band of 4.2 eV is formed by transitions from the VB to the donor level $\varepsilon_v$+4.2 eV [1,20,22]. The near-edge band of 4.65 eV is due to transitions from the VB to shallow donor levels [20].

### 3.2.2. *Influence of irradiation on film properties*

The effect of ion irradiation on the characteristics of the absorption spectra depends on the concentration of GDs and the degree of their interaction when combined into complexes with a continuous spectrum of levels. The processes of RDs accumulation and radiation-thermal annealing of defects in deposited amorphous and in annealed crystalline films are realized differently (Fig. 4).

The absorption centers in the deposited films have a less resistance to irradiation. Radiation-thermal annealing of GDs at doses of $\Phi \leq 2 \times 10^{14}$ $cm^{-2}$ shows a decrease in absorption in the range of $h\nu \leq 2.5$ eV, but an increase for levels at $h\nu$ = 3–4 eV (Fig. 4a and. 5a). The increase of defect generation rate $\Delta N/\Delta\Phi$ with the depth of their levels can be associated with the predominant generation of single RDs which are not bound into complexes (Fig. 5b). A slight decrease in the bandgap width from $E_g$' = 4.98 eV–4.97 eV at low ion doses $\Phi = (0.15–1.5) \times 10^{14}$ $cm^{-2}$ shows the radiation tolerance of the films (Table 1). The Urbach energy increase from $E_U$ = 0.19 eV–0.29 eV with increasing fluence up to $\Phi = 1.5 \times 10^{14}$ $cm^{-2}$ indicates enhanced interactions between deep levels of GDs and RDs. With increasing irradiation dose to $\Phi > 1.5 \times 10^{14}$ $cm^{-2}$, a continuous distribution of RDs levels is formed, which leads to a narrowing of the BG width to $E_g$' = 4.9 eV (Fig. 4a–Table 1). After irradiation, the local bands associated with GDs are generally preserved because the local bands of RDs have similar spectroscopic characteristics to GDs bands and their concentration is lower than the growth defects

**Table 1**
Electrical and optical characteristics of gallium oxide films.

| Φ, $cm^{-2}$ | Δ(hν), eV | $E_U$, eV | $E_g$', eV | $h\nu_{0(i)}$, eV | $N_{0(i)} \times 10^{16}$, $cm^{-3}$ | $б_d$, S | K, a.u. | $I_{PhS}$, A | $K_{UV}/K_{vis.}$ a.u. |
|---|---|---|---|---|---|---|---|---|---|
| Amorphous films (none-annealed) | | | | | | | | | |
| 0 | 4.5–5.1 | 0.19 | 4.98 | 2.6 | 12 | $2.0 \times 10^{-14}$ | 25–45 | $+1 \times 10^{-13}$ | 50 |
| | | | | 4.2 | 3.4 | | | | |
| | | | | 4.8 | 13 | | | | |
| $1.5 \times 10^{13}$ | 4.5–5.1 | 0.24 | 4.97 | 2.6 | 4.3 | $5 \times 10^{-15}$ | 1–2 | $-1 \times 10^{-12}$ | 12.5–20 |
| | | | | 4.2 | 30 | | | | |
| | | | | 4.8 | 59 | | | | |
| $1.5 \times 10^{14}$ | 4.5–5.1 | 0.29 | 4.97 | 2.6 | 2 | $1.2 \times 10^{-14}$ | 100–400 | $+8 \times 10^{-11}$ | 200–500 |
| | | | | 4.2 | 59 | | | | |
| | | | | 4.8 | 100 | | | | |
| $7.5 \times 10^{14}$ | 4.8–5.0 | 0.20 | 4.90 | 2.2 | 14 | $2.6 \times 10^{-14}$ | 100–170 | $-3 \times 10^{-12}$ | 200 |
| | 2.5–4.0 | 1.25 | – | 4.2 | 170 | | | | |
| | | | | 4.8 | 260 | | | | |
| Crystalline films (annealed at 900 °C) | | | | | | | | | |
| 0 | 1.2–4.7 | 1.3 | 4.77 | 3.6 | 160 | $2.5 \times 10^{-15}$ | 100–300 | – | 100 |
| | 4.5–5.1 | 0.33 | | | | | | | |
| $1.5 \times 10^{13}$ | – | – | – | 3.6 | 140 | $2 \times 10^{-15}$ | –(1–3) | $-4 \times 10^{-12}$ | 10 |
| $1.5 \times 10^{14}$ | – | – | – | 3.6 | 150 | $3 \times 10^{-15}$ | –(2–4) | $-2 \times 10^{-14}$ | 10 |
| $7.5 \times 10^{15}$ | 1.8–4.8 | 1.3 | 5.18 | 3.6 | 140 | $1.5 \times 10^{-15}$ | –(1–3) | $+1 \times 10^{-12}$ | 30–100 |
| | 5.1–5.3 | 0.15 | | | | | | | |

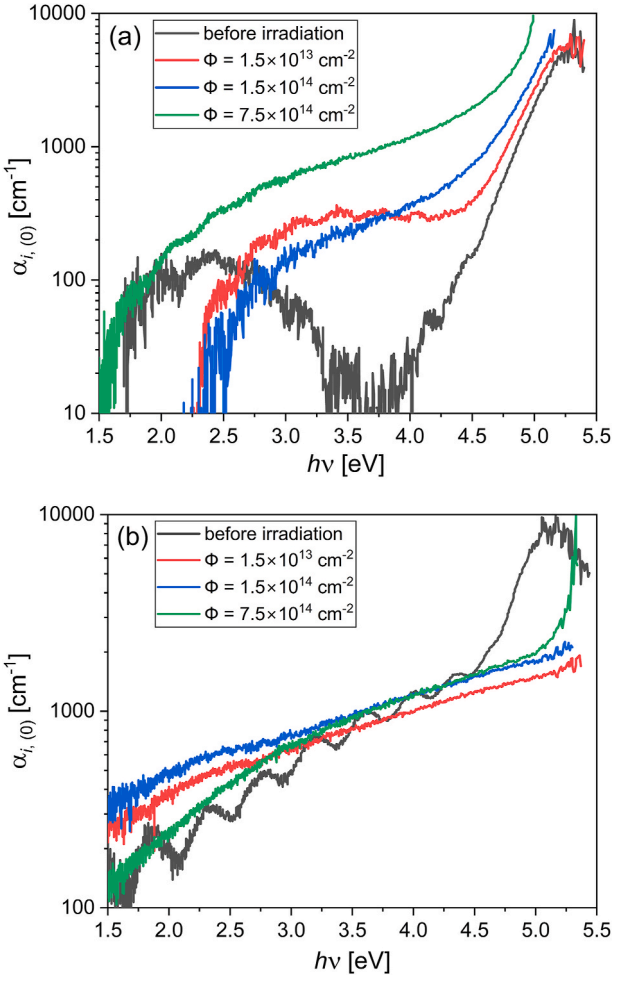


**Fig. 4.** Effect of short-pulsed ion irradiation on the spectral dependences of the absorption coefficient $\alpha_{i,(0)}(h\nu)$ of gallium oxide not annealed (a) and annealed (b) films.

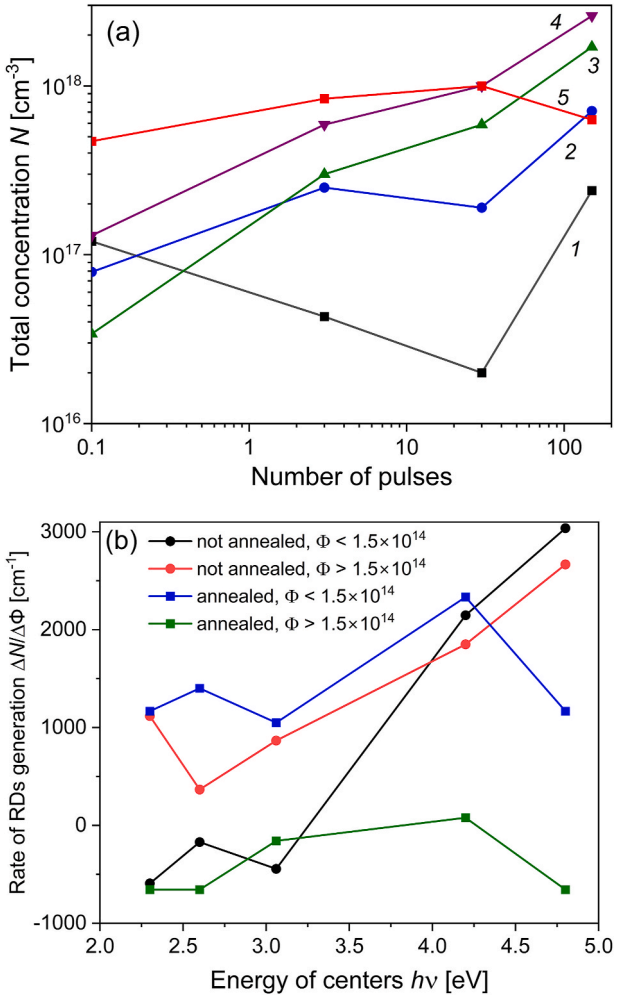


**Fig. 5.** (a) Influence of the number of irradiation pulses on the total concentration of absorption centers in gallium oxide films before (*1–4*) and after annealing (*5*) for hν = 2.6 eV (*1*, *5*), 3.06 eV (*2*), 4.2 eV (*3*) and 4.8 eV (*4*); (b) dependence of the defect injection rate $\Delta N/\Delta\Phi$ in none-annealed amorphous and in annealed crystalline films on the energy of the band centers $h\nu_{0(i)}$ for fluences $\Phi \leq 1.5 \times 10^{14}$ $cm^{-2}$ and $\Phi \leq 1.5 \times 10^{14}$ $cm^{-2}$.

(Figs. 3 and 6). At the same time, the edge band at 4.65 eV shifts to 4.8 eV. The RDs bands at 1.82 eV and 2.2 eV appear instead of the GDs 2.0 eV band after irradiation with $\Phi = 7.5 \times 10^{14}$ $cm^{-2}$. These changes in defect bands can be explained by the preferential accumulation of

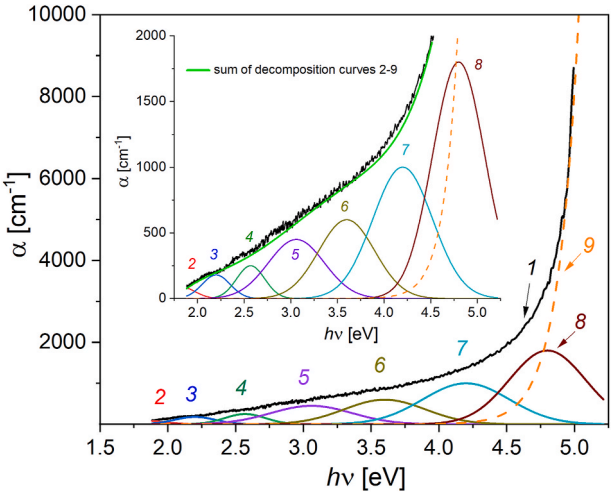


**Fig. 6.** Absorption spectrum α($h\nu$) of non-annealed films after irradiation with fluence of $\Phi = 7.5 \times 10^{14}$ cm$^{-2}$ (*1*) and its decomposition by Gaussians (*2–8*) with centers at $h\nu_0$ and half-with of γ: $h\nu = 1.82$ eV and γ = 0.15 eV (*2*), 2.2 eV and 0.15 eV (*3*), 2.6 eV and 0.15 eV (*4*), 3.06 eV and 0.3 eV (*5*), 3.6 eV and 0.3 eV (*6*), 4.2 eV and 0.32 eV (*7*), 4.8 eV and 0.28 eV (*8*). Curve (*9*) shows the fitting of absorption edge using Urbach rule with parameters $\alpha_{00} = 3 \times 10^{-11}$ cm$^{-1}$ and $E_U = 0.15$ eV.

anionic vacancies over cationic vacancies [20–23].

The absorption spectra of the irradiated crystalline β-$Ga_2O_3$ films and the kinetics of RDs accumulation indicate their higher radiation tolerance (Fig. 4a–. 5a and 7). As shown by the change in exponential and interband absorption characteristics, annealing of the films stimulates the formation of complexes from GDs that limit RDs formation. The weak dependence of the rate of RDs generation on their depth is due to the increased fraction of the continuous spectrum of localized states (Fig. 5b). The rate of RDs generation decreases significantly as the irradiation dose is increased.

The influence of radiation-thermal annealing becomes significant at $\Phi = 7.5 \times 10^{14}$ cm$^{-2}$ for RDs having shallow levels at 1.5–2.5 eV (Fig. 4b–. 5b and 8). Another remarkable effect of irradiation at $\Phi = 7.5 \times 10^{14}$ cm$^{-2}$ is the shift of the absorption edge by 0.3–0.4 eV to high energy area (Fig. 4b) and the increase of the BG width from $E_g = 4.77$ eV–5.18 eV with a corresponding decrease of the Urbach energy from $E_U$ = 0.33 eV–0.15 eV (Table 1). These changes in the parameters of interband and exponential absorption are determined by partial purification of the bandgap from shallow levels of GDs under the action of ions pulsed irradiation. The interaction between the levels of GDs and RDs

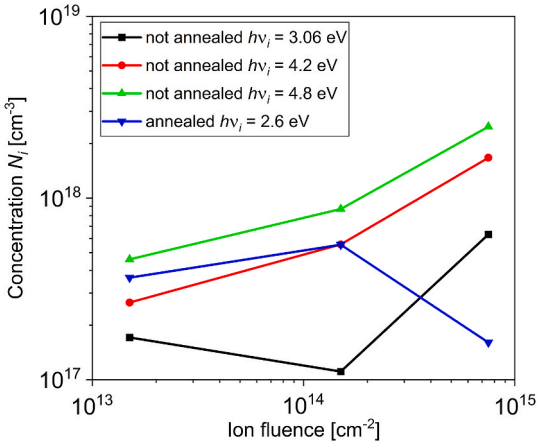


**Fig. 7.** Dependence of the RDs concentration $N_i$ on the fluence of ions Φ in gallium oxide films.

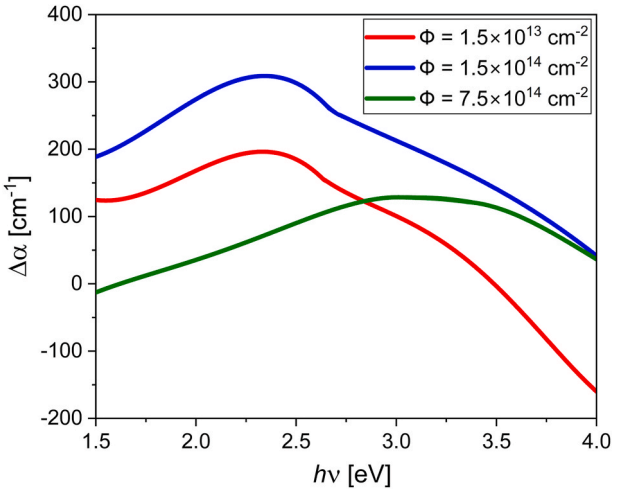


**Fig. 8.** Spectrum of induced absorption $\Delta\alpha_i(h\nu) = \alpha_i(h\nu) - \alpha_0(h\nu)$ in annealed gallium oxide films for different fluences of ions.

localized near the absorption edge is weakened, based on the dose dependence of $E_U(\Phi)$. The dominance of deeper levels as the ion dose accumulates is also observed in the interval of $h\nu \leq 4.0$ eV, as demonstrated by the difference absorption spectra $\Delta\alpha(h\nu) = \alpha_i(h\nu) - \alpha_0(h\nu)$, where $\alpha_0$ – absorption coefficient before and $\alpha_i$ – after irradiation (Fig. 8).

### 3.3. Photoluminescence

The observed 2–5 times increase in the intensity of photoluminescence of films after annealing at 900 °C is explained by annihilation of that part of growth defects, which serve as centers of radiation-free recombination in the deposited gallium oxide films. This is consistent with the facts of annealing of local absorption bands and formation of complexes with a continuous spectrum of absorption levels (Fig. 3 a, b). A similar change in luminescence has also been observed in MOCVD films [28].

The photoluminescence spectra of annealed β-$Ga_2O_3$ films contain bands centered at $h\nu_{0(i)}$ = 1.65, 2.05, 2.5, 2.95 and 3.3 eV, which characterize the β-$Ga_2O_3$ films obtained with different methods (Fig. 9) [28–33]. Photoluminescence bands at 2.66 and 3.41 eV were

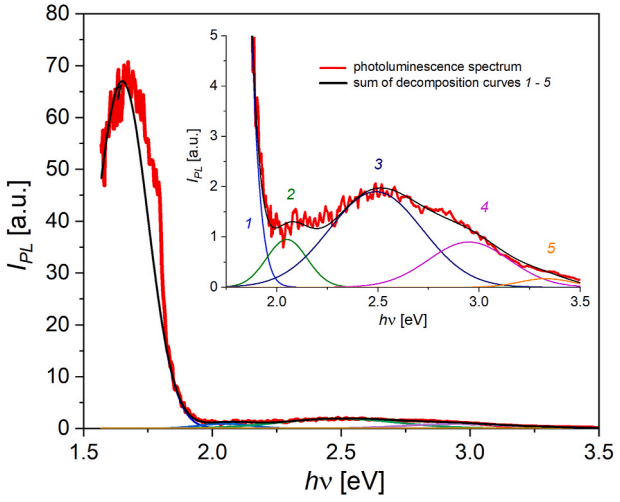


**Fig. 9.** Photoluminescence spectrum $I_{PL}(h\nu)$ of annealed gallium oxide films and its decomposition into Gaussians with parameters: $h\nu_{0(i)} = 1.67$ eV, $\gamma_i = 0.1$ eV (1); 2.05 eV, 0.1 eV (2): 2.5 eV, 0.23 eV (3); 2.95 eV, 0.16 eV (4) and 3.3 eV, 0.13 eV (5). The excitation energy was $h\nu = 4.96$ eV.

demonstrated in Ref. [24], and photoluminescence bands at 3.26, 2.98, 2.8 and 2.67 eV were found in β-$Ga_2O_3$ films deposited by magnetron sputtering [29]. A strong band at 1.65 eV is identified in Refs. [30,31].

We identified the origin of some photoluminescence bands in the deposited films by analogy with [20–44]. The weak photoluminescence band at 3.3 eV can be related to the nano-crystalline component of β-$Ga_2O_3$ by analogy with the work [32], although other bands at 2.61 and 3.75 eV are also exhibited in β-$Ga_2O_3$ nano-crystals [31]. In Ref. [34] the cathodoluminescence band of 3.25 eV was attributed to the recombination of free electrons with auto-localized holes. It is more likely that the band at 3.3 eV is associated with transitions in donor-acceptor pairs, where $V_{Ga}$ defects and/or $V_O$–$V_{Ga}$ complexes act as acceptors by analogy with [20,35]. We also cannot exclude the influence of localization of hole auto-captured polarons (by analogy with the band at 3.1 eV [36]) on it. The band at 2.95 eV can be due to transitions in donor-acceptor pairs from donor levels to that associated with $V_O$–$V_{Ga}$ complexes [1,26,34,37–41], or to levels of $V_{Ga}^{1-}$ [42]. The photoluminescence bands at 2.98, 2.8 and 2.67 eV according to Ref. [29] are identified with electronic transitions involving $V_O$ vacancy levels. The band of 2.5 eV can be related to transitions between the levels of intestinal $O_i^0$ defects considering the results of [42]. The band at 2.05 eV in view of theoretical calculations of [23,42] can be associated with transitions between $V_O^0$ vacancy levels. The band at 1.67 eV is probably due to the presence of the nano-crystalline component, but the contribution of transitions involving $V_O$ vacancy levels cannot be excluded [23,42]. This is supported by the established association of the 1.67 eV [43] and 1.75 eV [44] bands with the recombination of electrons captured by the $V_O$ donor with a hole localized on the acceptor associated with the doping of the material with nitrogen.

In irradiated films, the photoluminescence bands due to electron transitions involving the levels of growth defects at 1.67, 2.05, 2.5, 2.95, and 3.3 eV gradually disappeared with increasing in irradiation dose due to the capture of electrons from the levels of GDs to nearby RDs levels. The accumulation of absorption and non-radiative recombination centers corresponding to RDs dominates over the formation of luminescence centers. Kinetic parameters of induced absorption confirm this assumption (Figs. 5 and 7). The crystalline film after irradiation with a dose of $\Phi = 7.5 \times 10^{14}$ $cm^{-2}$ shows a single short-wavelength band at 3.74 eV, most likely due to intrinsic RDs (Fig. 10). The close in energy luminescence bands recorded in β-$Ga_2O_3$ crystal films at 3.75 eV [33], 3.2–3.6 eV [20], 3.65 eV [34], and 3.8 eV [22] were identified by the authors with transitions involving $V_O$ levels and donor-acceptor pairs and/or from allowed bands and $V_O$ levels. We suggest that the ion-induced 3.74 eV band is formed by recombination of holes from the valence band with electrons at the donor levels of the radiative $V_O$ by analogy to Refs. [20,22]. In general, the short-wavelength shift of photoluminescence after irradiation is consistent with absorption shifts in the intervals 4.5–5.2 eV and 2.0–4.0 eV (Figs. 4b and 6; Fig. 8) and corresponding changes in the exponential and interband absorption parameters (Table 1).

### 3.4. Photoelectric characteristics

#### 3.4.1. Electrical and photoelectric characteristics before irradiation

The deposited films are dielectric with the values of dark conductivity $\sigma_d \approx 2 \times 10^{-14}$ S and photoconductivity $\sigma_{ph} = (6.5–9) \times 10^{-13}$ S and photosensitivity $K = (\sigma_{ph}–\sigma_d)/\sigma_d = 25–45$. Annealing causes a decrease in dark conductivity and photoconductivity to $\sigma_d = (2–3) \times 10^{-15}$ S and $\sigma_{ph} = (4.0–8.5) \times 10^{-13}$ S, and an increase in photosensitivity to $K = 100–300$ and the appearance of its field dependence $K(U)$ (Fig. 11a and b).

The use of post-deposition annealing for the synthesis of β-$Ga_2O_3$ and annealing of GDs to enhance photoconductivity is widely known [1–4]. Also, for this purpose, increasing the deposition temperature [45–50] and control of the substrate material [51,52] are often used. In this case,

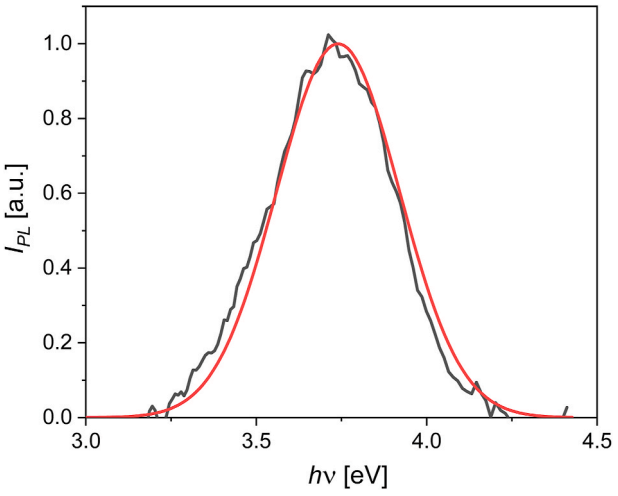


**Fig. 10.** Photoluminescence spectrum $I_{PL}(h\nu)$ of annealed gallium oxide films irradiated at fluence of $\Phi = 7.5 \bullet 10^{14}$ $cm^{-2}$ and its approximation by Gaussian with parameters $h\nu_0 = 3.74$ eV and $\gamma = 0.18$ eV. The excitation energy was $h\nu = 4.96$ eV.

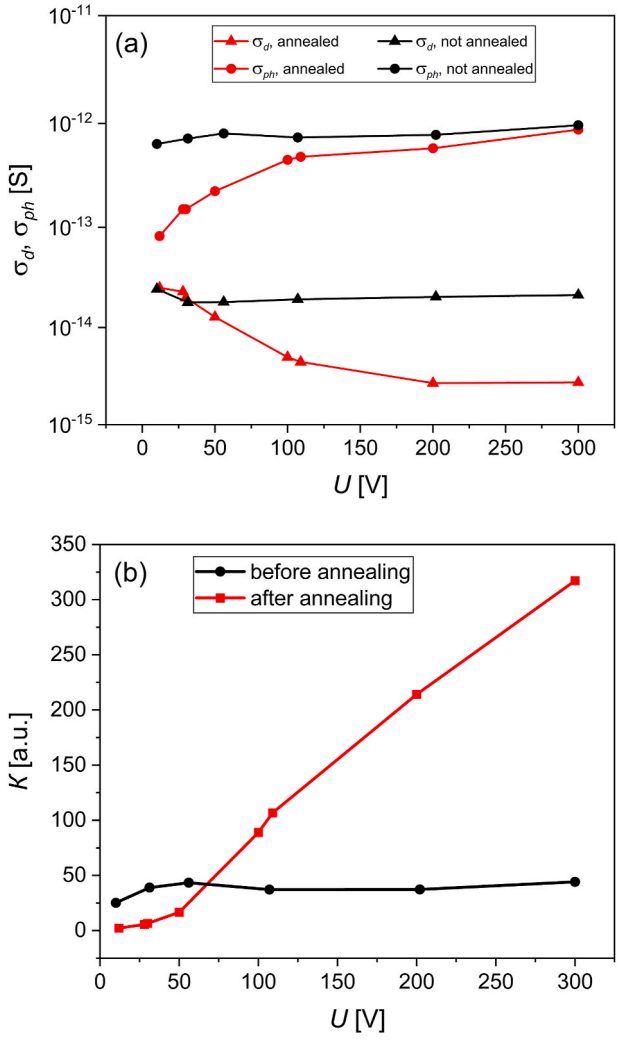


**Fig. 11.** (a) Dependences of surface dark conductivity ($\sigma_d$) and photoconductivity ($\sigma_{ph}$) of gallium oxide films before and after annealing on the applied voltage; (b) dependence of photosensitivity coefficient $K$ of films before and after annealing.

the type and concentration of growth defects (mainly $V_O$) play a significant role in the formation of the necessary kinetic and spectral characteristics of films, of course, not excluding the influence of structural parameters [46,48,53,54]. The strong field dependence of the photosensitivity is due to field transitions between photosensitive levels of different depths induced by growth defect complexes. On the contrary, the reason for greater stability of photosensitivity of amorphous films is the local character of optically and electrically active level defects (Fig. 11b). This is evidenced by absorption spectra (Figs. 3 and 4) and temperature dependences of $\sigma_d$ ($T$) ($T$ = 300–400 K), which are characterized by peaks due to thermal activation of deep energy levels $\varepsilon_\sigma$ = 1.42–1.45 eV (Fig. 12). These local levels of charge carrier transfer centers are probably associated with defects of the acceptor type, namely $V_{Ga}^{+(0)}$, which is confirmed by the positive sign of photostimulated currents $I_{PhS} = +1 \times 10^{-13}$ A (Table 1) [55]. Trapping of charge carriers excited by light to deep acceptor levels suppresses the photosensitivity of non-annealed films in general. During annealing, non-useful defects annihilate and/or are converted into complexes, which contributes to photosensitivity.

### 3.4.2. Radiation effect

Short-pulsed ion irradiation of films is inevitably accompanied by competing processes of defect accumulation and annihilation, which occurs due to rapid heating of the near-surface layers to high temperatures of 1300–1500 K within a short time of $10^{-6}$–$10^{-5}$ s and subsequent cooling [12,16].

The change in the field dependences of $\sigma_{d(ph)}$(U), $K$(U), and the sign of photostimulated currents $I_{PhS}(\Phi)$, showing the predominant type of RDs, is clearly observed in the none-annealed films (Figs. 13a and 14 and Table 1). A sharp decrease in the dark conductivity, photoconductivity and photosensitivity after irradiation of amorphous films with a small dose $\Phi = 1.5 \times 10^{13}$ cm$^{-2}$ is accompanied by the introduction of photosensitive defects of donor type, as shown by negative sign of $I_{PhS} = -1 \times 10^{-12}$ A (Fig. 13a–Table 1). At the same time, the absorption spectra testify to the annihilation of growth defects, which correspond to levels distributed in the low energy range of 1.5–2.6 eV (Fig. 4a and. 5a). Apparently, the introduction of such RDs downgrades the ratio of photosensitivity in the UV and visible ranges to value of $K_{UV}/K_{vis}$ = 12.5–20 (Table 1). In the second stage of irradiation at $\Phi > 1.5 \times 10^{14}$ cm$^{-2}$, the accumulation of RDs clearly dominates their annihilation. This is expressed in the increase of dark conductivity and photoconductivity (Fig. 13a). Photosensitivity increases and it has a field

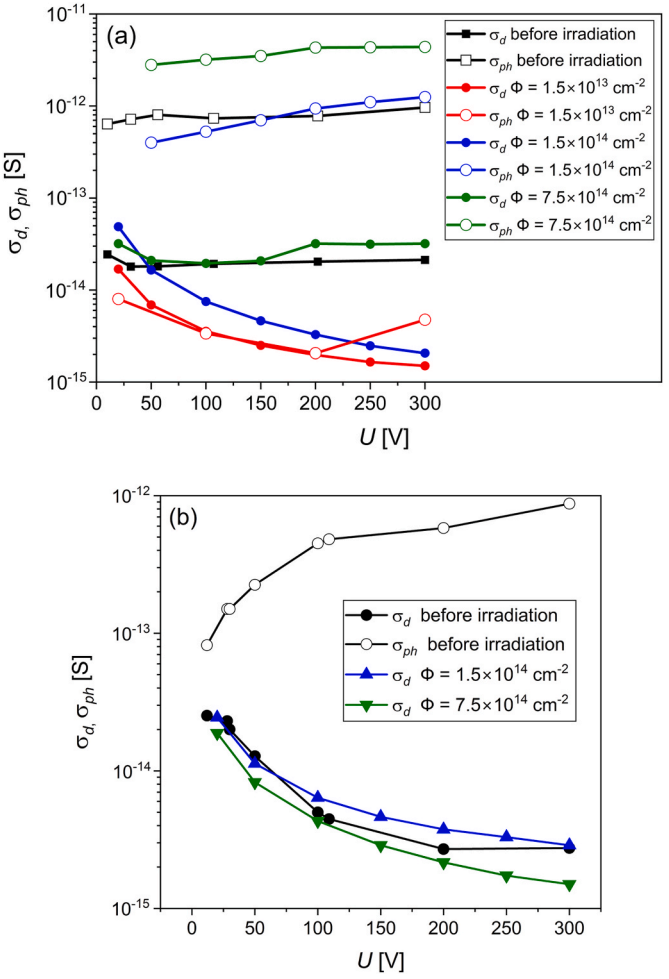


**Fig. 13.** (a) Dependences of the dark conductivity $\sigma_d$ and photoconductivity $\sigma_{ph}$ from voltage in the gallium oxide films none-annealing before and after short-pulse ion irradiation at fluences $\Phi = 1.5 \times 10^{13}$ cm$^{-2}$, $1.5 \times 10^{14}$ cm$^{-2}$ and $7.5 \times 10^{14}$ cm$^{-2}$; (b) dependences of the dark conductivity $\sigma_d$ and photoconductivity $\sigma_{ph}$ from voltage in the gallium oxide films annealed at 900 °C before and after short-pulsed ion irradiation at fluences $\Phi = 1.5 \times 10^{14}$ cm$^{-2}$ and $7.5 \times 10^{14}$ cm$^{-2}$.

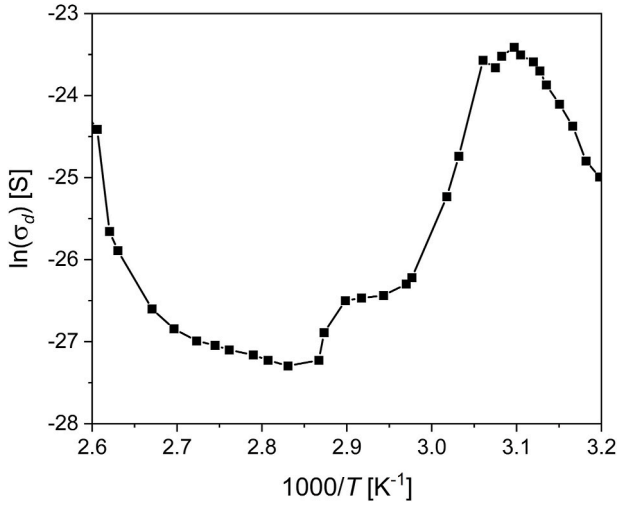


**Fig. 12.** Temperature dependence of dark conductivity $\sigma_d$ of gallium oxide films before annealing. The voltage at the electrodes is $U$ = 100 V. The distance between the electrodes is 0.2–0.3 cm and the electrode length is 0.5 cm. The conduction activation energy $\varepsilon_\sigma$ = 1.42–1.45 eV.

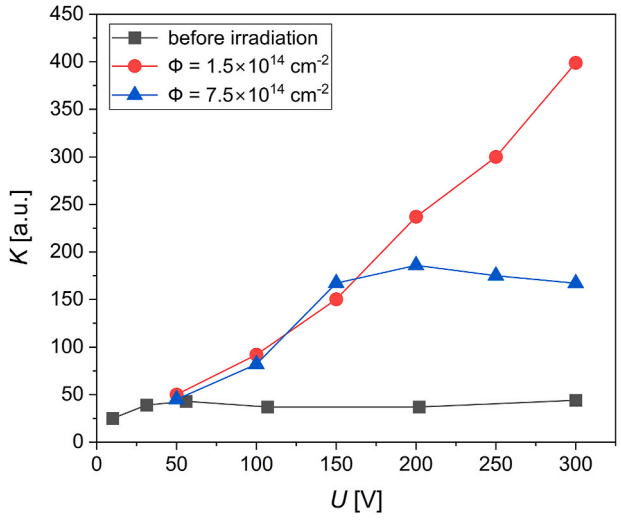


**Fig. 14.** Effect of short-pulse ion irradiation on the photosensitivity coefficient $K$ of non-annealed amorphous films.

dependence (Fig. 14). At the same time, the ratio of photosensitivity in the UV and visible ranges improves to $K_{UV}/K_{vis}$ = 200–500 (Table 1). The type of photo-generated charge carriers changes first to hole ($I_{PhS}$ = + 8 × $10^{-11}$ A) at Φ = 1.5 × $10^{14}$ $cm^{-2}$ and then to electron ($I_{PhS}$ = – 3 × $10^{-12}$ A) at Φ = 7.5 × $10^{14}$ $cm^{-2}$, indicating the unstable nature of the kinetics of donor- and acceptor-type RDs accumulation (Table 1). The similar increase in photocurrent was observed after neutron irradiation, which was attributed to an increase in the density of deep acceptors in the lower half of the bandgap due to $V_{Ga}$ [49]. Prevailing accumulation of donor RDs over acceptor RDs at Φ = 7.5 × $10^{14}$ $cm^{-2}$ is associated with redistribution of induced absorption to the high-energy region (Fig. 4a).

In annealed crystalline films under the same irradiation conditions no additional post-radiation conductivity is created, and photosensitivity even has negative values (Fig. 13b–Table 1). This correlates with the enhancement of the continuous component in the absorption spectra (Fig. 4b). The bands at 1.6 eV, 2.4–2.6 eV, and 3.6 eV in the spectra of induced absorption $\Delta\alpha_i(h\nu)$ are associated with transition between the RDs levels (Fig. 8). These levels can serve as charge carrier trapping centers, which suppresses photoconductivity. The generation of donor RDs prevails, as shown by photostimulated currents $I_{PhS}(\Phi)$, but at Φ = 7.5 × $10^{14}$ $cm^{-2}$ the photoconductivity changes from electronic to hole (Table 1), which correlates with the short-wavelength band shift in the $\Delta\alpha_i(h\nu)$ spectra (Fig. 8) and the appearance of a short-wavelength photoluminescence band at 3.74 eV connected with RDs, namely $V_O$ (Fig. 10).

## 4. Conclusion

The gallium oxide thin films deposited on α-$Al_2O_3$ (0001) substrates by reactive magnetron sputtering were amorphous dielectric with relatively low photo-sensitivity. Annealing the films in air at 900 °C forms a β-$Ga_2O_3$ phase in films with grainsizes about 20 nm and partially improves their characteristics.

Short-pulsed ion irradiation by 200 keV carbon ions and protons of deposited non-annealed gallium oxide thin films with fluences Φ = (0.15–1.5) × $10^{14}$ $cm^{-2}$ slight decreases the bandgap width from 4.98 eV to 4.97 eV, which indicates high radiation resistance of amorphous films. At ion fluences of Φ = 7.5 × $10^{14}$ $cm^{-2}$, the bandgap narrows significantly to 4.9 eV, which shows a continuous distribution of radiation defect levels. For annealed films at ion fluences of Φ = 7.5 × $10^{14}$ $cm^{-2}$, the bandgap width increases to 5.18 eV while the Urbach energy value decreases to 0.15 eV. This phenomenon indicates a decrease in concentration of growth defects having the shallow levels after radiation-thermal effect of beam. The irradiation decreases the intensity of luminescence bands due to the capture of electrons from the levels of growth defects to the nearby levels of radiation defects.

The annealing decreases the dark conductivity and photo conductivity to values of $\sigma_d$ = (2–3) × $10^{-15}$ S and $\sigma_{ph}$ = (4.0–8.5) × $10^{-13}$ S, and the photosensitivity increases to $K$ = 100–300 compared to $K$ = 25–45 for the non-annealed films, due to the β-$Ga_2O_3$ phase formation, the annihilation of unstable defects and/or conversion of single defects into complexes. After irradiation with a dose of Φ = 1.5 × $10^{13}$ $cm^{-2}$, a decrease in dark, photoconductivity and photosensitivity is observed for amorphous and crystalline films. Conversely, at irradiation dose Φ = 1.5 × $10^{14}$ $cm^{-2}$, an increase in dark and photoconductivity is observed, which shows the predominance of the accumulation of radiation defects over their annihilation. The photoelectrical characteristics of amorphous films demonstrates higher radiation resistance to short-pulsed ion irradiation, compared to annealed films. Moreover, irradiation at a dose higher than 1.5 × $10^{14}$ $cm^{-2}$ stimulates an increase in the photosensitivity of amorphous films and a decrease the sensitivity to visible light due to the introduction of deep photosensitive levels of acceptor radiation defects in the bandgap.

## CRediT authorship contribution statement

**Zhanymgul Koishybayeva:** Writing – original draft, Visualization, Supervision, Resources, Project administration, Investigation, Funding acquisition, Conceptualization. **Fedor Konusov:** Writing – original draft, Visualization, Resources, Investigation. **Sergey Pavlov:** Writing – original draft, Visualization, Supervision, Resources, Project administration, Investigation, Conceptualization. **Dmitrii Sidelev:** Writing – review & editing, Resources, Investigation. **Artur Nassyrbayev:** Resources, Investigation. **Dmitry Cheshev:** Writing – review & editing, Visualization, Resources, Investigation. **Ruslan Gadyrov:** Resources, Investigation. **Vladislav Tarbokov:** Resources, Investigation. **Abdirash Akilbekov:** Resources, Funding acquisition.

## Funding

This research was funded by the Ministry of Science and Higher Education of the Republic of Kazakhstan (Grant No. AP14972907). The work of F. Konusov, S. Pavlov, V. Tarbokov was performed in the framework of a State Task in the area of scientific activity (agreement FSWW-2023-0011).

## Declaration of competing interest

The authors declare that they have no known competing financial interests or personal relationships that could have appeared to influence the work reported in this paper.

## Data availability

Data will be made available on request.

## References

[1] S.J. Pearton, J. Yang, P.H. Cary, et al., A review of $Ga_2O_3$ materials, processing, and devices, Appl. Phys. Rev. 5 (2018) 011301, https://doi.org/10.1063/1.5006941.
[2] J. Xu, W. Zheng, F. Huang, Gallium oxide solar-blind ultraviolet photodetectors: a review, J. Mater. Chem. C 7 (2019) 8753–8770, https://doi.org/10.1039/C9TC02055A.
[3] X. Chen, F. Ren, S. Gu, J. Ye, Review of gallium-oxide-based solar-blind ultraviolet photodetectors, Photon. Res. 7 (2019) 381–415, https://doi.org/10.1364/PRJ.7.000381.
[4] D. Kaur, M. Kumar, A strategic review on gallium oxide based deep-ultraviolet photodetectors: recent progress and future prospects, Adv. Opt. Mater. 9 (2021) 2002160, https://doi.org/10.1002/adom.202002160.
[5] W. Drozdowski, M. Makowski, A. Bachiri, M.E. Witkowski, A.J. Wojtowicz, L. Swiderski, K. Irmscher, R. Schewski, Z. Galazka, Heading for brighter and faster β-Ga2O3 scintillator crystals, Opt. Mater. X 15 (2022) 100157, https://doi.org/10.1016/j.omx.2022.100157.
[6] A. Luchechko, V. Vasyltsiv, L. Kostyk, O. Tsvetkova, A.I. Popov, Shallow and deep trap levels in X-ray irradiated β-Ga2O3: Mg, Nucl. Instrum. Methods Phys. Res. Sect. B Beam Interact. Mater. Atoms 441 (2019) 12–17, https://doi.org/10.1016/j.nimb.2018.12.045.
[7] Y. Suchikova, A. Lazarenko, S. Kovachov, A. Usseinov, Z. Karipbaev, A.I. Popov, Formation of porous $Ga_2O_3$/GaAs layers for electronic devices. 2022 IEEE 16th International Conference on Advanced Trends in Radioelectronics, Telecommunications and Computer Engineering (TCSET), 2022, pp. 1–4, https://doi.org/10.1109/TCSET55632.2022.9766890. Lviv-Slavske, Ukraine.
[8] A. Usseinov, A. Platonenko, Z. Koishybayeva, A. Akilbekov, M. Zdorovets, A. I. Popov, Pair vacancy defects in β-$Ga_2O_3$ crystal. Ab initio study, Opt. Mater. X 16 (2022) 100200.
[9] A.B. Usseinov, Z.T. Karipbayev, J. Purans, A.B. Kakimov, A. Bakytkyzy, A. M. Zhunusbekov, T.A. Koketai, A.L. Kozlovskyi, Y. Suchikova, A.I. Popov, Study of β-$Ga_2O_3$ ceramics synthesized under powerful electron beam, Materials 16 (2023) 6997, https://doi.org/10.3390/ma16216997.
[10] Y. Suchikova, S. Kovachov, I. Bohdanov, D. Drozhcha, I. Kosogov, Z.T. Karipbayev, A.I. Popov, Synthesis and characterization of β-$Ga_2O_3$/por-GaAs/mono-GaAs heterostructures for enhanced portable solar cells, Physics and Chemistry of Solid State 25 (2024) 546–552, https://doi.org/10.15330/pcss.25.3.546-552.
[11] Y. Suchikova, S. Kovachov, I. Bohdanov, I. Kosogov, D. Drozhcha, A.I. Popov, Design and structural characteristics of $Ga_2O_3$/por-GaAs/mono-GaAs Heterostructures for Advanced MEMS Applications. IEEE 19th International Conference on the Perspective Technologies and Methods in MEMS Design (MEMSTECH), 2024, pp. 48–51, https://doi.org/10.1109/MEMSTECH63437.2024.10620009.

[12] J. Kim, S.J. Pearton, C. Fares, J. Yang, F. Ren, S. Kim, A.Y. Polyakov, Radiation damage effects in $Ga_2O_3$ materials and devices, J. Mater. Chem. C 7 (2019) 10–24, https://doi.org/10.1039/C8TC04193H.

[13] S. Ahn, Y.H. Lin, F. Ren, S. Oh, Y. Jung, G. Yang, J. Kim, M. Mastro, J. Hite, C. R. Eddy, S.J. Pearton, Effect of 5 MeV proton irradiation damage on performance of β-$Ga_2O_3$ photodetectors, J. Vac. Sci. Technol. B 34 (2016) 041213, https://doi.org/10.1116/1.4950872.

[14] A. Azarov, V. Venkatachalapathy, E.V. Monakhov, A.Y. Kuznetsov, Dominating migration barrier for intrinsic defects in gallium oxide: dose-rate effect measurements, Appl. Phys. Lett. 118 (2021) 232101, https://doi.org/10.1063/5.0051047.

[15] G. Remnev, V. Tarbokov, S. Pavlov, F. Konusov, S. Zenkin, J. Musil, Irradiation of sputtered Al-Si-N coatings by pulsed 200 keV C+ ion beam, Vacuum 158 (2018) 65–67, https://doi.org/10.1016/j.vacuum.2018.09.022.

[16] F. Urbach, The long-wavelength edge of photographic sensitivity and of the electronic absorption of solids, Phys. Rev. 92 (1953) 1324, https://doi.org/10.1103/PhysRev.92.1324.

[17] D.L. Dexter, Absorption of light by atoms in solids, Phys. Rev. 101 (1956) 48–55, https://doi.org/10.1103/PhysRev.101.48.

[18] C. Kranert, C. Sturm, R. Schmidt-Grund, M. Grundmann, Raman tensor elements of β-$Ga_2O_3$, Sci. Rep. 6 (2016) 35964, https://doi.org/10.1038/srep35964.

[19] F. Konusov, S. Pavlov, A. Lauk, A. Kabyshev, V. Novikov, R. Gadirov, G. Remnev, Effect of short-pulsed ion irradiation on the optical and electrical properties of titanium nitride films deposited by reactive magnetron sputtering, Nucl. Instrum. Methods Phys. Res. Sect. B Beam Interact. Mater. Atoms 526 (2022) 51–59, https://doi.org/10.1016/j.nimb.2022.06.011.

[20] Zh Wang, X. Chen, F.-F. Ren, Sh Gu, J. Ye, Deep-level defects in gallium oxide, J. Phys. Appl. Phys. 54 (2021) 043002, https://doi.org/10.1088/1361-6463/abbeb1.

[21] Z. Zhang, E. Farzana, A.R. Arehart, S.A. Ringel, Deep level defects throughout the bandgap of (010) β-$Ga_2O_3$ detected by optically and thermally stimulated defect spectroscopy, Appl. Phys. Lett. 108 (2016) 052105, https://doi.org/10.1063/1.4941429.

[22] H. Gao, S. Muralidharan, N. Pronin, Md R. Karim, S.M. White, T. Asel, G. Foster, S. Krishnamoorthy, S. Rajan, L.R. Cao, M. Higashiwaki, Wenckstern H. von, M. Grundmann, H. Zhao, D.C. Look, L.J. Brillson, Optical signatures of deep level defects in $Ga_2O_3$, Appl. Phys. Lett. 112 (2018) 242102, https://doi.org/10.1063/1.5026770.

[23] J.B. Varley, J.R. Weber, A. Janotti, C.G. Van de Walle, Oxygen vacancies and donor impurities in β-$Ga_2O_3$, Appl. Phys. Lett. 97 (2010) 142106, https://doi.org/10.1063/1.3499306.

[24] K. Yamanaka, H. Raebiger, K. Mukai, K. Shudo, Modulation of the optical absorption edge of ε- and κ-$Ga_2O_3$ due to Co impurities caused by band structure changes: work function measurements and first-principle calculations, J. Appl. Phys. 127 (2020) 065701, https://doi.org/10.1063/1.5134521.

[25] A.Y. Polyakov, V.I. Nikolaev, I.N. Meshkov, K. Siemek, P.B. Lagov, E.B. Yakimov, A.I. Pechnikov, O.S. Orlov, A.A. Sidorin, S.I. Stepanov, I.V. Shchemerov, A. A. Vasilev, A.V. Chernykh, A.A. Losev, A.D. Miliachenko, I.A. Khrisanov, Yu S. Pavlov, U.A. Kobets, S.J. Pearton, Point defect creation by proton and carbon irradiation of α-$Ga_2O_3$, J. Appl. Phys. 132 (2022) 035701, https://doi.org/10.1063/5.0100359.

[26] M.D. Heinemann, J. Berry, G. Teeter, T. Unold, D. Ginley, Oxygen deficiency and Sn doping of amorphous $Ga_2O_3$, Appl. Phys. Lett. 108 (2016) 022107, https://doi.org/10.1063/1.4938473.

[27] M. Orita, H. Hiramatsu, H. Ohta, M. Hirano, H. Hosono, Preparation of highly conductive, deep ultraviolet transparent β-$Ga_2O_3$ thin film at low deposition temperatures, Thin Solid Films 411 (2002) 134–139, https://doi.org/10.1016/S0040-6090(02)00202-X.

[28] H.W. Kim, N.H. Kim, Influence of postdeposition annealing on the properties of $Ga_2O_3$ films on $SiO_2$ substrates, J. Alloys Compd. 389 (2005) 177–181, https://doi.org/10.1016/j.jallcom.2004.05.082.

[29] L. Dong, R. Jia, B. Xin, B. Peng, Y. Zhang, Effects of oxygen vacancies on the structural and optical properties of β-$Ga_2O_3$, Sci. Rep. 7 (2017) 40160, https://doi.org/10.1038/srep40160.

[30] T. Zhang, J. Lin, X. Zhang, Y. Huang, X. Wu, Y. Xue, J. Zou, Ch Tang, Single-crystalline spherical β-$Ga_2O_3$ particles: synthesis, N-doping and photoluminescence properties, J. Lumin. 140 (2013) 30–37, https://doi.org/10.1016/j.jlumin.2013.02.031.

[31] X.T. Zhou, F. Heigl, J.Y.P. Ko, M.W. Murphy, J.G. Zhou, T. Regier, R.I.R. Blyth, T. K. Sham, Origin of luminescence from $Ga_2O_3$ nanostructures studied using x-ray absorption and luminescence spectroscopy, Phys. Rev. B Condens. Matter 75 (2007) 125303, https://doi.org/10.1103/PhysRevB.75.125303.

[32] L.L. Liu, M.K. Li, D.Q. Yu, J. Zhang, H. Zhang, C. Qian, Z. Yang, Fabrication and characteristics of N-doped β-$Ga_2O_3$, Appl. Phys. A 98 (2010) 831–835, https://doi.org/10.1007/s00339-009-5538-y.

[33] C.H. Liang, G.W. Meng, G.Z. Wang, Y.W. Wang, L.D. Zhang, S.Y. Zhang, Catalytic synthesis and photoluminescence of nanowires, Appl. Phys. Lett. 78 (2001) 3202, https://doi.org/10.1063/1.1374498.

[34] J. Lee, E. Flitsiyan, L. Chernyak, J. Yang, F. Ren, S.J. Pearton, B. Meyler, Y. J. Salzman, Effect of 1.5 MeV electron irradiation on β-$Ga_2O_3$ carrier lifetime and diffusion length, Appl. Phys. Lett. 112 (2018) 082104, https://doi.org/10.1063/1.5011971.

[35] T. Onuma, S. Fujioka, T. Yamaguchi, M. Higashiwaki, K. Sasaki, T. Masui, T. Honda, Correlation between blue luminescence intensity and resistivity in β-$Ga_2O_3$ single crystals, Appl. Phys. Lett. 103 (2013) 041910, https://doi.org/10.1063/1.4816759.

[36] K.A. Mengle, G. Shi, D. Bayerl, E. Kioupakisa, First-principles calculations of the near-edge optical properties of β-$Ga_2O_3$, Appl. Phys. Lett. 109 (2016) 212104, https://doi.org/10.1063/1.4968822.

[37] S. Li, S. Jiao, D. Wang, S. Gao, J. Wang, The influence of sputtering power on the structural, morphological and optical properties of β-$Ga_2O_3$ thin films, J. Alloys Compd. 753 (2018) 186–191, https://doi.org/10.1016/j.jallcom.2018.04.196.

[38] Q. Shi, Q. Wang, D. Zhang, Q. Wang, Sh Li, W. Wang, Q. Fan, J. Zhang, Structural, optical and photoluminescence properties of $Ga_2O_3$ thin films deposited by vacuum thermal evaporation, J. Lumin. 206 (2019) 53–58, https://doi.org/10.1016/j.jlumin.2018.10.005.

[39] I.D. Hosein, M. Hegde, P.D. Jones, V. Chirmanov, P.V. Radovanovic, Evolution of the faceting, morphology and aspect ratio of gallium oxide nanowires grown by vapor–solid deposition, J. Cryst. Growth 396 (2014) 24–32, https://doi.org/10.1016/j.jcrysgro.2014.03.037.

[40] H.M. Lam, M.H. Hong, S. Yuan, T.C. Chong, Growth of β-$Ga_2O_3$ nanoparticles by pulsed laser ablation technique, Appl. Phys. A 79 (2004) 2099, https://doi.org/10.1007/s00339-004-2893-6.

[41] M.D. McCluskey, Point defects in $Ga_2O_3$, J. Appl. Phys. 127 (2020) 101101, https://doi.org/10.1063/1.5142195.

[42] Q.D. Ho, T. Frauenheim, P. Deák, Origin of photoluminescence in β-$Ga_2O_3$, Phys. Rev. B 97 (2018) 115163, https://doi.org/10.1103/PhysRevB.97.115163.

[43] Y.P. Song, H.Z. Zhang, C. Lin, Y.W. Zhu, G.H. Li, F.H. Yang, D.P. Yu, Luminescence emission originating from nitrogen doping of β-$Ga_2O_3$ nanowires, Phys. Rev. B 69 (2004) 075304, https://doi.org/10.1103/PhysRevB.69.075304.

[44] S. Kumar, C. Tessarek, S. Christiansen, R. Singh, A comparative study of β-$Ga_2O_3$ nanowires grown on different substrates using CVD technique, J. Alloys Compd. 587 (2014) 812–818, https://doi.org/10.1016/j.jallcom.2013.10.165.

[45] Y. Kokubun, K. Miura, F. Endo, S. Nakagomi, Sol-gel prepared thin films for ultraviolet photodetectors, Appl. Phys. Lett. 90 (2007) 031912, https://doi.org/10.1063/1.2432946.

[46] A.Y. Polyakov, V.I. Nikolaev, S.A. Tarelkin, A.I. Pechnikov, S.I. Stepanov, A. E. Nikolaev, I.V. Schhemerov, E.B. Yakimov, N.V. Luparev, M.S. Kuznetsov, A. A. Vasilev, A.I. Kochkova, M.I. Voronova, M.P. Scheglov, J. Kim, S.J. Pearton, Electrical properties and deep trap spectra in $Ga_2O_3$ films grown by halide vapor phase epitaxy on p-type diamond substrates, J. Appl. Phys. 129 (2021) 185701, https://doi.org/10.1063/5.0044531.

[47] Y. Xu, Z. An, L. Zhang, Q. Feng, J. Zhang, C. Zhang, Y. Hao, Solar blind deep ultraviolet β-$Ga_2O_3$ photodetectors grown on sapphire by the Mist-CVD method, Opt. Mater. Express 8 (2018) 334158, https://doi.org/10.1364/OME.8.002941.

[48] Y. Li, T. Tokizono, M. Liao, M. Zhong, Y. Koide, I. Yamada, J.J. Delaunay, Efficient assembly of bridged β-$Ga_2O_3$ nanowires for solar-blind photodetection, Adv. Funct. Mater. 20 (2010) 3972, https://doi.org/10.1002/adfm.201001140.

[49] S. Ghose, Sh Rahman, L. Hong, J.S. Rojas-Ramirez, H. Jin, K. Park, R. Klie, R. Droopad, Growth and characterization of β-$Ga_2O_3$ thin films by molecular beam epitaxy for deep-UV photodetectors, J. Appl. Phys. 122 (2017) 095302, https://doi.org/10.1063/1.4985855.

[50] F.P. Yu, S.L. Ou, D.S. Wuu, Pulsed laser deposition of gallium oxide films for high performance solar-blind photodetectors, Opt. Mater. Express 5 (2015) 1240–1249, https://doi.org/10.1364/OME.5.001240.

[51] J. Yu, Y. Wang, H. Li, Y. Huang, W. Tang, Z. Wu, Tailoring the solar-blind photoresponse characteristics of β-$Ga_2O_3$ epitaxial films through lattice mismatch and crystal orientation, J. Phys. Appl. Phys. 53 (2020) 24LT01, https://doi.org/10.1088/1361-6463/ab7e67.

[52] M.Q. Li, N. Yang, G.G. Wang, H.Y. Zhang, J.C. Han, Highly preferred orientation of $Ga_2O_3$ films sputtered on SiC substrates for deep UV photodetector application, Appl. Surf. Sci. 471 (2019) 694–702, https://doi.org/10.1016/j.apsusc.2018.12.045.

[53] S.J. Hao, M. Hetzl, F. Schuster, K. Danielewicz, A. Bergmaier, G. Dollinger, Q.L. Sai, C.T. Xia, T. Hoffmann, M. Wiesinger, S. Matich, W. Aigner, M. Stutzmann, Growth and characterization of β-$Ga_2O_3$ thin films on different substrates, J. Appl. Phys. 125 (2019) 105701, https://doi.org/10.1063/1.5061794.

[54] K. Kikuchi, S. Imura, K. Miyakawa, H. Ohtake, M. Kubota, E. Ohta, Photocurrent multiplication in $Ga_2O_3$/$CuInGaSe_2$ heterojunction photosensors, Sensor Actuator Phys. 224 (2015) 24–29, https://doi.org/10.1016/j.sna.2015.01.001.

[55] A.Y. Polyakov, N.B. Smirnov, I.V. Shchemerov, S.J. Pearton, F. Ren, A.V. Chernykh, T.V. Kulevoy, Hole traps and persistent photocapacitance in proton irradiated β-$Ga_2O_3$ films doped with Si, Apl. Mater. 6 (2018) 096102, https://doi.org/10.1063/1.5042646.